Tuning of the Excited-State Properties and Photovoltaic Performance in PPV-Based Polymer Blends

Chunhong Yin,[†] Marcel Schubert,[†] Sebastian Bange,[†] Burkhard Stiller,[†] Mauro Castellani,[†] Dieter Neher,*[,†] Michael Kumke,[‡] and Hans-Heinrich Hörhold[§]

Institute of Physics and Astronomy, University of Potsdam, Karl-Liebknecht-Strasse 24-25, 14476 Golm, Germany, Institute of Chemistry, University of Potsdam, Karl-Liebknecht-Strasse 24-25, 14476 Golm, Germany, and Institute of Organic Chemistry and Macromolecular Chemistry, University of Jena, Humboldtstrasse 10, 07743 Jena, Germany

Received: May 6, 2008; Revised Manuscript Received: June 24, 2008

The authors use solvents with different boiling points and a mixture of these solvents to tune the morphology of blends formed from poly[2,5-dimethoxy-1,4-phenylenevinylene-2-methoxy-5-(2-ethylhexyloxy)-1,4-phenylenevinylene] (M3EH-PPV) and poly[oxa-1,4-phenylene-1,2-(1-cyano)-ethylene-2,5-dioctyloxy-1,4-phenylene-1,2-(2-cyano)-ethylene-1,4-phenylene] (CN-ether-PPV). In photoluminescence (PL), the emission of as-prepared films spin-coated from chloroform (CF) is entirely dominated by an exciplex, with no evidence for the radiative decay of either the M3EH-PPV or the CN-ether-PPV exciton. Evidently these intrachain excited species dissociate rapidly by intermolecular charge transfer, pointing to a highly intermixed blend morphology. On the other hand, the PL of films deposited from 1,2,4-trichlorobenzene (TCB) exhibits predominant emission from the M3EH-PPV exciton, indicating the presence of rather pure M3EH-PPV domains in the phase-separated polymers layers. The blend morphology is shown to have a large influence on the solar cell properties and particularly on the fill factor. For an annealed layer coated from a 1:4 TCB:CF mixture, a fill factor of 44% was achieved, which is among the highest values reported for polymer−polymer blends. For all blends the photocurrent rises linearly with light intensity, implying that bimolecular recombination and the formation of space charge from the photogenerated carriers is of minor importance. Charge carrier mobilities and bimolecular recombination coefficients were measured on the very same polymer blends used for solar cell fabrication, utilizing the method of "charge carrier extraction by linearly increasing voltage technique" (photo-CELIV). These studies did not reveal a significant effect of the blend morphology on the bulk carrier transport and recombination. The authors conclude that the photovoltaic properties are mainly determined by processes on the very local scale, namely the competition between the field-induced dissociation and recombination of the initially formed polaron pairs. It is proposed that the nanomorphology has a profound effect on the initial separation of these Coulombically bound electron−hole pairs and on the probability that they recombine via the formation of interfacial exciplexes or, possibly, via intrachain triplet excitons.

1. Introduction

Solution-processed solar cells fabricated from conjugated polymers have attracted increasing attention due to their low-cost manufacturing. In addition, the high optical absorption coefficient of the polymers allows fabricating of ultra thin photovoltaic cells, which will in turn considerably reduce their cost and weight. A challenge in organic photovoltaic devices is to achieve efficient charge separation of electrons and holes created upon photon absorption. A revolutionary development was the introduction of blend systems in the mid 1990s.[1−3] By blending two derivatives of poly(*p*-phenylene vinylene) (PPV), a phase-segregated interpenetrating net work was formed and thereby increased the interfacial area dramatically, and the possibility for an exciton to reach the interface and dissociate was largely increased.

State of the art solar cells made from polymer−polymer blends exhibit energy conversion efficiencies (ECEs) on the order of 1.5−1.8%.[4−6] Those values are distinctly lower than those reported from blends of polymers with the electron acceptor [6,6]-phenyl-C_{61}-butyric acid methyl ester (PCBM).[7−9] One general observation is that the fill factor (FF) of all-polymer blend devices seldom exceeds 40%, meaning that the number of photogenerated charges extracted from the device depends significantly on the internal electric field. Those low FFs have often been attributed to inefficient transport and extraction of photogenerated carriers to the electrodes.[10]

We recently studied the photovoltaic properties of devices made from poly[2,5-dimethoxy-1,4-phenylenevinylene-2-methoxy-5-(2-ethylhexyloxy)-1,4-phenylenevinylene] (M3EH-PPV) and poly[oxa-1,4-phenylene-1,2-(1-cyano)-ethylene-2,5-dioctyloxy-1,4-phenylene-1,2-(2-cyano)-ethylene-1,4-phenylene] (CN-ether-PPV) (see Scheme 1 for chemical structures). Optimized solar cells made from a blend of these two PPV derivatives had an ECE of 1.7% (FF = 35%, J_{sc} = 3.57 mA/cm^2, V_{oc} = 1.36 V).[4,11] By comparing the photocurrent characteristics of bilayer and blend devices, we could unambiguously show that bimolecular recombination and charge extraction do not compromise device performance, leaving the field-dependence of charge carrier generation as the main reason for the low FF.[12,13]

* Corresponding author. Address: Universität Potsdam, Institut für Physik and Astronomie, Karl-Liebknecht-Strasse 24-25, Haus 28, 14476 Potsdam.
[†] Institute of Physics, University of Potsdam.
[‡] Institute of Chemistry, University of Potsdam.
[§] University of Jena.

10.1021/jp803977k CCC: $40.75
Published on Web 08/22/2008

SCHEME 1: Chemical structures of the electron donor polymer M3EH-PPV and electron acceptor polymer CN-Ether-PPV

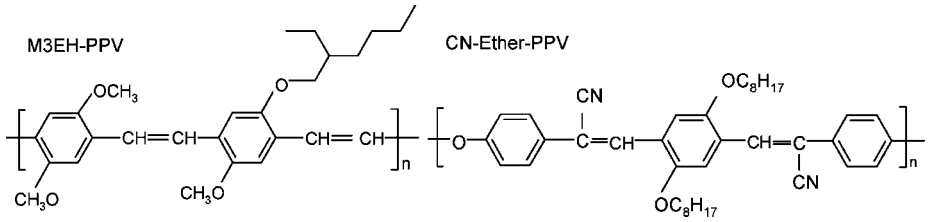

This picture is in agreement with conclusions drawn from studies on polymer−PCBM blends by Mihailetchi et al.[14] Our recent study also addressed the reason for the significant improvement in efficiency upon annealing of the polymer blend. One remarkable finding was a strict anticorrelation between the photocurrent and the intensity of long wavelength exciplex emission in the photoluminescence (PL) spectra of the blend layers. It was proposed that annealing leads to a higher degree of phase separation, which in turn increases the probability for the dissociation of electron−hole pairs bound at the heterojunction into free carriers. Similar conclusions have been drawn recently by McNeill et al. and Mandoc et al. from studies on other polymer−polymer blend systems.[15,16] Apparently, the efficiency of free carrier generation is strongly related to the exact nanomorphology of the sample and a certain degree of demixing is a necessary condition for achieving high efficiencies in polymer-based solar cells.

It is well established that the type of solvent used for spin coating, the spin rotation speed, and the solution concentration have a significant influence on the polymer blend morphology. Solvents with different boiling points will result in different drying times during the film formation, thus affecting the morphology and the photovoltaic properties of the polymer blend device[17,18] Furthermore, different solubilities of the two components in a common solvent affect the phase separation during drying of the layer. For example, additives that selectively dissolve only one component were shown to improve the efficiency of solar cells made from a polymer−PCBM blend.[19,20]

In an effort to extend the understanding of the interrelation between structural, optical, and optoelectronic properties in polymer−polymer photovoltaic devices, we have performed studies on M3EH-PPV:CN-ether-PPV blends coated from different solvents as well as from a solvent mixture. We compared M3EH-PPV:CN-ether-PPV (1:1 by weight) blends prepared from 1,2,4-trichlorobenzene (TCB), chloroform (CF), and mixtures of TCB and CF with respect to the PL, morphology, and solar cell performance. CF is a good solvent for both polymers, while TCB is a selective solvent for CN-ether-PPV, implying that M3EH-PPV will first solidify upon drying of the layer. A second reason why we selected TCB is its high boiling point (∼230 °C) owing to its low vapor pressure (0.29 mmHg at 25 °C).[21] Film formation from TCB will therefore be rather slow, which allows the polymer chains to reorganize themselves during evaporation of the solvent. Studies on polymer-based field transistors have shown superior performance for layers coated from this high boiling point solvent, which was attributed to a highly ordered chain morphology.[22] For these two reasons, a phase-separated morphology is expected even in the as-prepared blend layers coated from TCB.

2. Experimental Section

Materials. M3EH-PPV (M_w = 44 kg/mol) and CN-ether-PPV (M_w = 20.6 kg/mol) were provided by Prof. Hörhold, Jena. The poly(ethylene dioxythiophene) doped with polystyrene sulfonic acid (PEDOT:PSS) was purchased from HC Starck (Al4083). All chemicals were used as received without further purification.

Device Preparation. M3EH-PPV:CN-ether-PPV (1:1 by weight) blends were coated either from the pure solvents CF (8 g/L), CB (13 g/L), or TCB (18 g/L), or from a mixture of TCB and CF with different weight ratios (10 g/L). The solubilities of the two polymers differ strongly in the three solvents. CN-ether-PPV dissolves easily in all three pure solvents, while M3EH-PPV is well soluble only in CF. In order to obtain a clear M3EH-PPV solution in TCB or the TCB:CF mixture, the solution needed to be heated at 80 °C for 10 min with subsequent sonification for 15 min.

For all solar cell devices, an approximately 50 nm thin layer of PEDOT:PSS was spin-coated onto commercially available glass substrates covered with indium tin oxide (ITO, 13 Ω/square). The PEDOT:PSS films were dried under nitrogen atmosphere for 30 min at 110 °C. Then the M3EH-PPV:CN-ether-PPV blend was cast directly on the PEDOT−PSS. After coating, the layers were either baked in nitrogen atmosphere at 130 °C (above the T_g of both polymers) for 30 min (annealed samples), or dried at room temperature at 10^{-1} mbar for 12 h (as-prepared samples). If not stated otherwise, the final layer thickness was about 60 nm, as determined with a surface profilometer (Dektak 3ST).

The devices were completed by evaporating a 30 nm Ca layer protected by 100 nm Al at a pressure of 1×10^{-6} mbar. The effective solar-cell area as defined by the geometrical overlap between the bottom ITO electrode and the top cathode was ca. 0.20 cm^2. All device preparation and characterization was performed under nitrogen atmosphere.

Device Characterization. The external quantum efficiency (incident photon-to-converted electron efficiency (IPCE)) of the devices was measured with a homemade setup. An Oriel 150W Xe-lamp combined with an Oriel Cornerstone 260 monochromator gave the desired wavelength. The number of photons incident on the samples was calculated at each wavelength by using a calibrated Si-diode (SN1316). The current−voltage characteristics were recorded under illumination with a Steuernagel solar simulator at a light power density of ca. 90 mW/cm^2. A Keithley 2400 was used for applying the bias voltage and recording the current. For studying the dependence of the photocurrent on the incident light intensity, different neutral density filters were placed between the sample and the white light source. The resulting light intensity was inferred from the product of the original light intensity and the transmission of the used gray filters.

Optical Spectroscopy. Steady-state fluorescence spectra were measured with Perkin-Elmer LS55 luminescence spectrometers. Time-resolved PL studies were performed using a single photon-counting setup. The samples were excited with a frequency-doubled titanium:sapphire laser (Tsunami, Spectra Physics) at

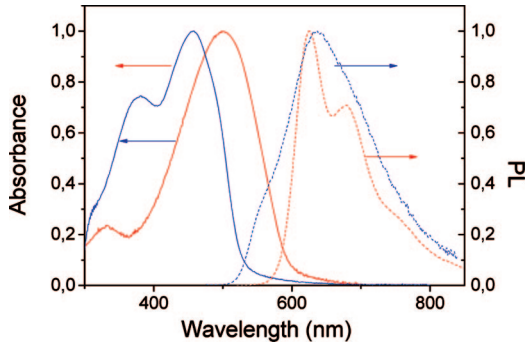

Figure 1. Normalized absorbance (solid line) and PL (dashed line) spectra of M3EH-PPV (red) and CN-Ether-PPV (blue) films coated from chlorobenzene (CB).

a wavelength of 405 nm, at which both the donor and acceptor polymer absorb. Fluorescence spectra were measured with a FL920 fluorometer (Edinburgh Instruments, Livingston, U.K.). The complete detection system had an instrumental response time of 100 ps. For data analysis and deconvolution of the instrument-response function, the commercial software package provided with the FL920 fluorescence spectrometer was used. To determine the actual time resolution of the setup, Xanthion was measured in different solvents and the PL transients were compared to those obtained by detection with a streak camera (Hamamatsu). From these studies, the time resolution was estimated to be ca. 30 ps.[23] Note that the samples for time-resolved PL measurement had a slightly different architecture from the solar cell devices. The polymer was deposited directly onto oxygen plasma-treated glass substrates. The sample was either dried in vacuum at room temperature or annealed at 130 °C for 30 min. Then a 200 nm thick silver layer was thermally deposited on top of the polymer film to protect it from oxygen and water. Finally the sample was sealed with a second glass slide on top of the silver layer by using a UV curable glue (ACW, AC A1438).

3. Results and Discussion

3.1. PL Studies. Before discussing the emission properties of the blend films, we would like to briefly review the optical properties of the corresponding pure polymer layers. M3EH-PPV has a well-resolved emission spectrum with the maximum at 600 nm. The transient PL of the film is characterized by a biexponential decay with a lifetime of 0.4 and 0.7 ns (not shown here). Both observations suggest that the emission is due to the radiative decay of an intrachain singlet exciton. Note that Chasteen et al. published a faster single-exponential decay for a layer of M3EH-PPV with a lifetime of 0.3 ns,[24] which slightly differs from our finding. According to our knowledge, the M3EH-PPV polymer used in their study is from a different batch and differs in molecular weight. The excited-state properties of CN-ether-PPV have been studied by Chasteen et al. and found to be similar to those of the well-known CN-PPV.[25] While the emission of the polymer in solution is due to an intrachain exciton (with the emission peak at 550 nm), it is dominated by an interchain excimer in the solid state. The emission of the film as shown in Figure 1 is characterized by a broad featureless band extending from 520 nm into the near-infrared (NIR), centered at ca. 605 nm. The weak shoulder at ca. 550 nm can be attributed to the CN-ether-PPV intrachain exciton. The decay at long wavelength is originated from the recombination of the excimer. It is multiexponential with decay times of 3.0 ns (36%), 7.9 ns (61%), and 0.5 ns (3%) at 600 nm (while Chasteen et al. reported decay times of 3.5 ns (33%) and 11.0 ns (66%)).

Figure 2 shows normalized steady state PL spectra excited at 500 nm for as-prepared and annealed blend layers coated from pure TCB and CF. Also shown are the respective spectra for a layer cast from CB. As reported previously, the PL spectrum of the blend coated from CB exhibits a broad peak centered at ca. 680 nm in addition to emission from the M3EH-PPV exciton (note that the PL spectra of CB-cast films reported earlier by us[4,12,26] were not properly calibrated in the red and NIR wavelength region). Broad and red-shifted emission spectra have recently been reported for a variety of blends of electron-donating and electron-accepting polymers and attributed to an interchain exciplex.[24,25,27−30] It is believed that these exciplexes form either directly upon dissociation of an intrachain exciton or via a "dark" polaron pair.

For our blends coated from CB, exciplex emission can be excited at 550 nm (at which only the M3EH-PPV absorbs), and its relative intensity increases when using shorter excitation wavelengths (Figure 3). Apparently, exciplex formation occurs via either the M3EH-PPV or the CN-ether-PPV exciton. There is no noticeable emission below 550 nm (even when exciting the sample at the absorption maximum of CN-ether-PPV), implying that the exciton on the electron acceptor is fully quenched in the blend. The shape of the overall spectra remains the same for all excitation wavelengths. Therefore, emission from the CN-ether-PPV excimer must be very weak. As pointed out by Chasteen et al., the very long lifetime of both the exciton and the excimer in CN-ether-PPV will make these species particularly vulnerable to be quenched.[25]

In contrast, the as-prepared CF-cast film features only the 680 nm exciplex peak, with no evidence for excitonic emission from either M3EH-PPV or CN-ether-PPV. When moving the excitation to shorter wavelength, the overall emission intensity increases due to additional absorption by the electron-acceptor, but the shape of the PL spectrum stays the same. Apparently, excitons formed on either CN-ether-PPV or M3EH-PPV rapidly decay to form exciplexes, indicating a high degree of intermixing in the as-prepared samples coated from CF. No evidence for excimer emission can be seen in the steady-state PL spectra. Since both polymers are very soluble in CF, blends made therefrom are expected to become homogeneously intermixed on a molecular level. In addition, the rapid evaporation of CF prevents phase separation upon drying. Upon annealing, the exciplex intensity is reduced, and the emission from the M3EH-PPV exciton becomes visible, indicating the formation of a phase-separated structure.

For as-prepared samples coated from TCB, the singlet exciton and exciplex emission bands are of similar intensity (for excitation at 550 nm). The emission spectrum barely changes upon annealing. This gives strong evidence that the blend morphology is phase-separated and close to an equilibrium state right after spin-coating. The PL spectra of films spin coated from different ratios of TCB and CF are compared in Figure 4. With increasing CF fraction, the exciplex emission raises continuously, indicating that the morphology becomes more and more intermixed.

We would like to point out that the optical data presented here do not allow one to differentiate whether exciton dissociation and exciplex formation occurs at the interface between a pure donor and a pure acceptor phase or within individual phases. Flory−Huggins theory predicts that phases formed by the demixing of two polymers are not pure but contain minority components. There is no doubt that such nanoscale intermixing occurs in blends of the two most studied polyfluorenes, poly(9,9′-dioctylfluorene-*co*-bis-*N*,*N*′-(4-butylphenyl)-bis-*N*,*N*′-

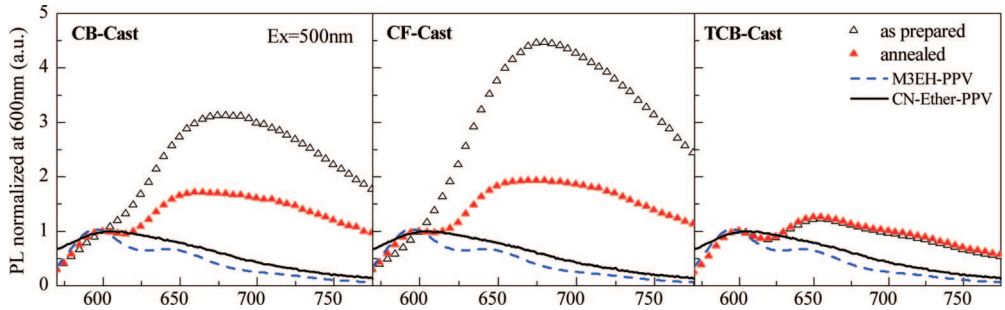

Figure 2. The PL spectra for films of 1:1 M3EH-PPV:CN-ether-PPV blends spin-coated from pure solvents. The open symbols show results obtained from as-prepared layers, and the filled symbols represent data measured on annealed layers. All the samples were prepared on plain glass substrates and excited at 500 nm. For comparison, the PL of pure M3EH-PPV (dashed line) and CN-ether-PPV (solid line) is also shown. The thickness of all blend layers was ca. 80 nm. The spectra are normalized for the same emission intensity at 600 nm.

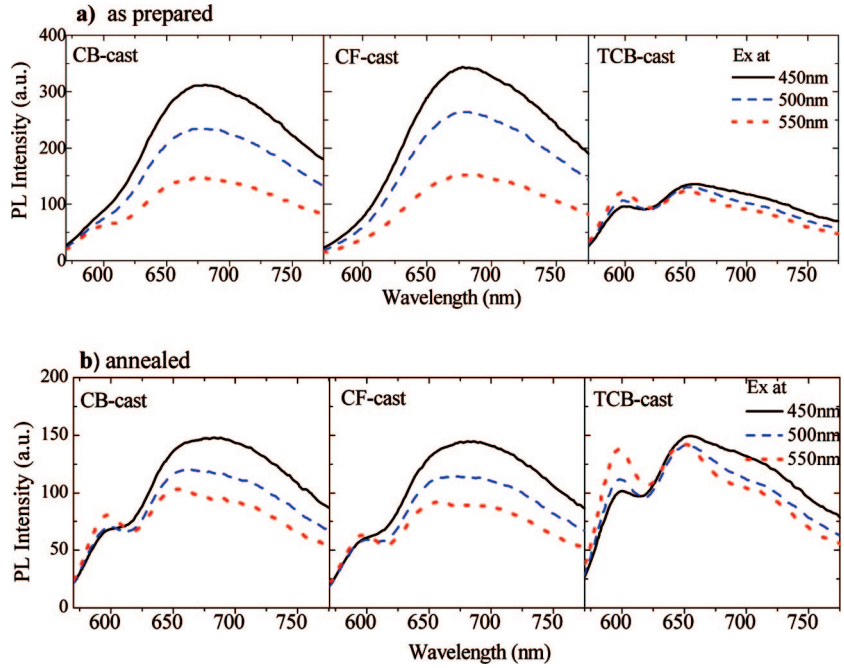

Figure 3. PL spectra of 1:1 M3EH-PPV:CN-ether-PPV blends excited at different wavelengths. The films had a thickness of ca. 80 nm. The spectra have been calibrated for the same excitation intensity.

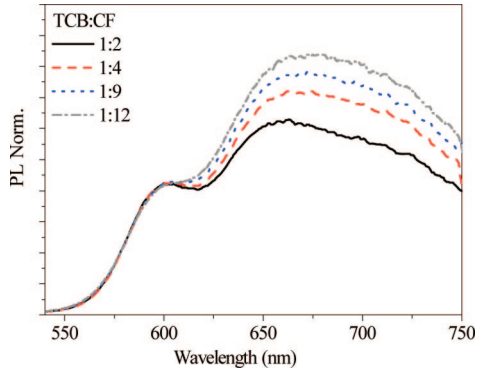

Figure 4. Normalized PL spectra of as-prepared M3EH-PPV:CN-ether-PPV (1:1 by weight) blend films spin-coated from TCB/CF solvent mixtures for different ratios. The samples were excited at 500 nm.

phenyl-1,4-phenylenediamine) (PFB) and poly(9,9′-dioctylfluorene-*co*-benzothiadiazole) (F8BT).[31,32] Our recent studies on the optical properties of PFB:F8BT blends formed in nanoparticles further revealed that exciton emission is mainly from the F8BT-rich phase (with an PFB concentration of less than 5 wt %), while exciplex formation occurs mainly in the PFB-rich phase (with a 10−15% F8BT minority content).[33] On the other hand, recent work by McNeill and co-workers suggested that the domains in annealed PFB:F8BT blend layers have a high purity.[16] For the studied M3EH-PPV:CN-ether-PPV blend, we are not in possession of information on the purity of the phases.

3.2. Morphology Studies. Unfortunately, layers cast from pure TCB were rather inhomogeneous and not useful for device fabrication. Quite homogeneous films could be obtained when the CF ratio in the mixed solvent was 80% and above. For this composition, the relative emission intensity at 680 nm is still significantly lower than that for the CB-coated layers. Figure 5 depicts the atomic force microscopy (AFM) topography images of 1:1 M3EH-PPV:CN-ether-PPV films spin-coated from a 1:4 mixture of TCB and CF or from CF. For films cast from TCB/CF, the surface is relatively rough on a submicrometer scale, with a root-mean-square (rms) roughness of ca. 2.7 nm. In contrast, as prepared films cast from CF have a very smooth surface, with an rms roughness of below 1 nm. These observations are consistent with the picture extracted from the optical studies. Apparently, as-prepared layers casted from CF exhibit a homogeneous blend morphology, while layers coated from the solvent mixtures possess nanosized domains. A similar behavior was also observed by Li et al. in their studies on the self-organization of polythiophene/fullerene blend system where

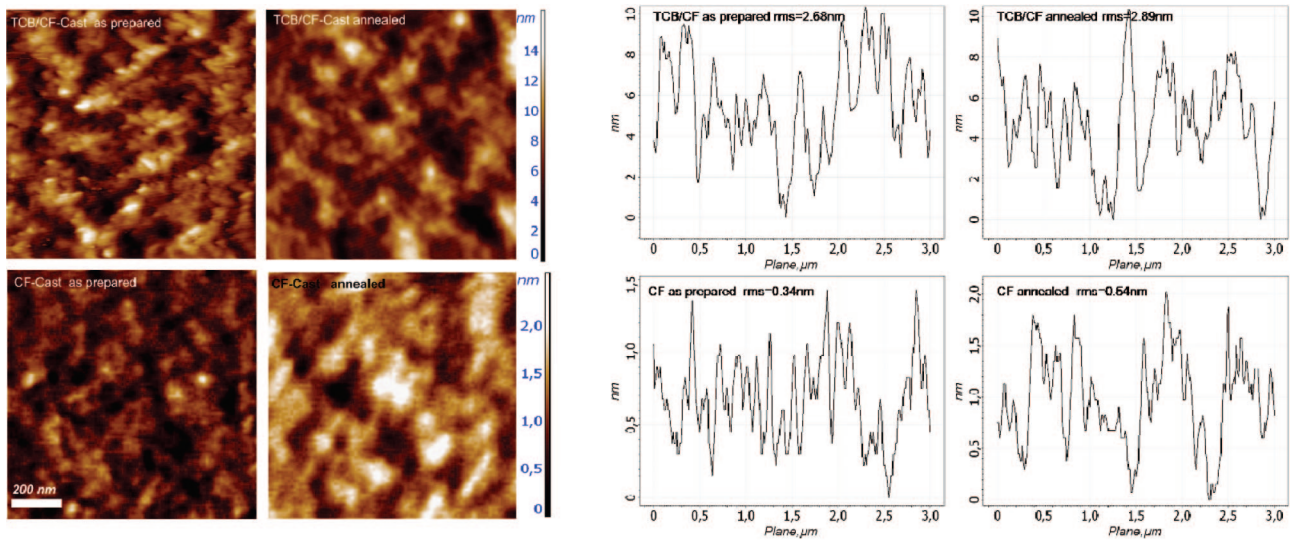

Figure 5. Tapping-mode AFM topography images of 1:1 M3EH-PPV:CN-ether-PPV blends spin-coated from TCB/CF (1:4) or from pure CF. Typical height profiles obtained from these images are shown on the right side.

they pointed out that the rough surface of slow-grow film is a signature of polymer self-organization to ordered structures in the film.[7]

3.3. Time-Resolved PL Studies. All PL spectra except those measured on the as-prepared blend coated from CB exhibit a clear contribution from the M3EH-PPV exciton. This emission might arise either from the radiative decay of initially photoexcited excitons or from excitons "recycled" from exciplexes through thermal excitation. The latter process was first proposed by Morteani et al.[27] for polyfluorene blends and recent work supported the view that this process is also active in PPV-based blends.[24,34] To improve the understanding of the excited-state properties in relation to the blend morphology, PL decay measurements were performed on the as-prepared and the annealed samples.

Transient decays measured on layers cast from CF and the TCB/CF solvent mixture are plotted on a log−log scale in Figure 6. The curves have been normalized to the same PL intensity at a transient time of 4 ns. The corresponding semilog decay curves are included as an inset in every diagram.

For a detection wavelength of 700 nm, contributions from intrachain excitons on either component must be very weak, and the emission shall be dominated by the exciplex (with a possible weak emission contribution from the excimer on CN-ether-PPV). The decay curves are almost biexponential, but the fit is further improved by including a small decay component with very short decay time. Noticeably, the decay of the as-prepared blend coated from CF is nearly monoexponential, with a decay time of 3.3 ns (see Table 1). This suggests that the as-prepared blend from CF is a rather homogeneous mix of the two components. We therefore attribute the 3.3 ns component to the decay of an exciplex localized on adjacent polymer chains. Note that Chasteen et al. originally assigned a 3.5 ns decay to the intrachain exciton on CN-ether-PPV.[24] Because of the very low PL intensity below 550 nm (at which the CN-ether-PPV exciton emits), we can safely exclude this assignment.

For all other samples, the PL decays at 700 nm consist of a shorter component of 1.7−2 ns (51−61%) and a longer decay with 5.2−6.1 ns (28−33%). The presence of two decay components in all blends with significant phase separation might be caused by the larger inhomogeneity of the layers and might even indicate that exciplex emission stems from two distinct phases (either rich in M3EH-PPV or in CN-ether-PPV).

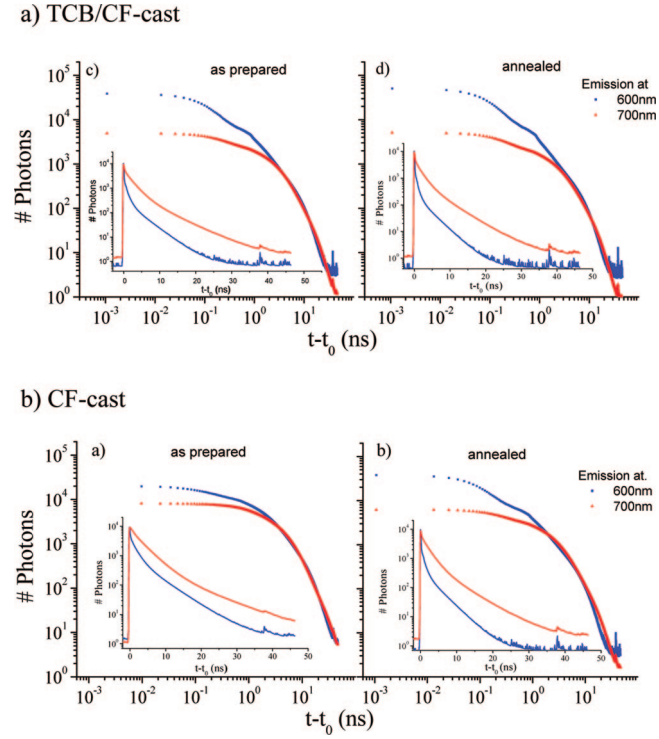

Figure 6. Time-resolved PL transients (double-log representation) for polymer blend films prepared from a 1:4 TCB/CF mixture (a) or from pure CF (b). Samples were excited at 405 nm and the emission was detected at 600 or 700 nm. The insets show the decays on a semilog scale.

At 600 nm, the emission from the exciplex is negligible weak. The decays are clearly triexponential. Except for the as-prepared CF-cast film, they show essentially the same dynamic features: a very fast decay (60−70 ps, 42−60%), an intermediate component (0.75−0.88 ns, 21−29%), and a slow decay (3.4−3.9 ns, 20−29%). Following the interpretation by Chasteen et al. the fast component is assigned to the intrachain exciton formed in the M3EH-PPV-rich phase, which is rapidly quenched by dissociation in the blend. The rather high yield of the initial fast component indicates that the excitonic contribution seen in the steady-state PL spectra stems mainly from initially generated excitons. It further implies that the length scale of

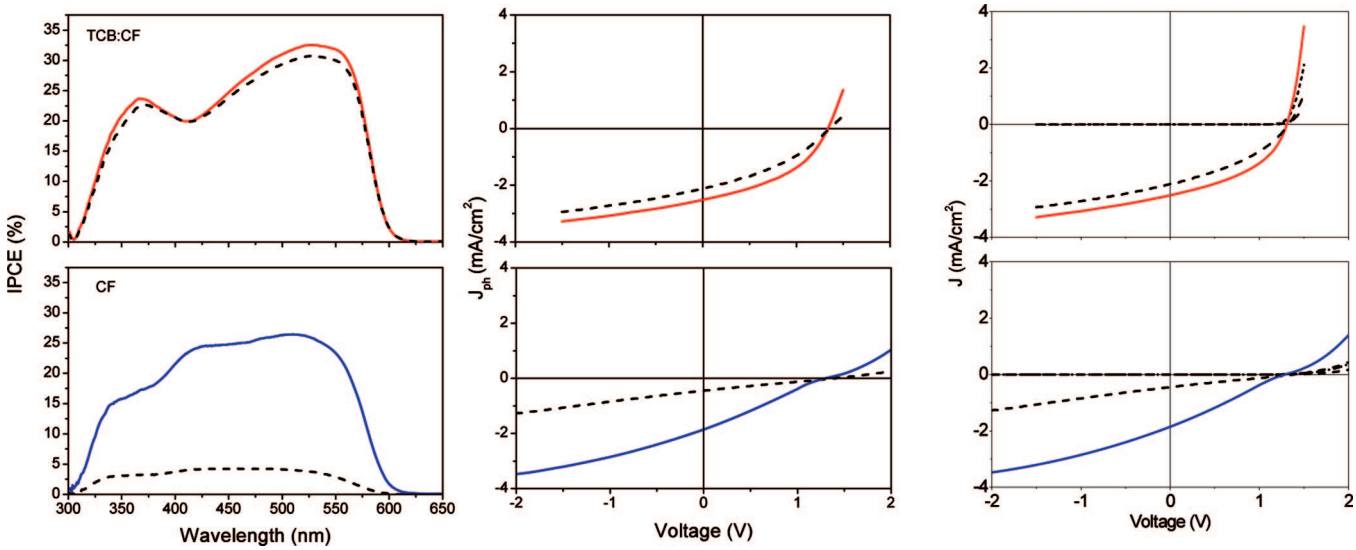

Figure 7. Photovoltaic properties of M3EH-PPV:CN-ether-PPV (1:1) blend devices. The active layers were spin-coated either from TCB/CF (1:4) or from CF. From left to right is the external quantum efficiency vs wavelength, the photocurrent-density vs voltage, and the current density vs voltage under illumination or in the dark. The solid lines represent the annealed devices, and the black dashed lines show the as-prepared devices. Dark current densities are plotted as black dash-dotted lines. The current−voltage characteristics were measured under AM1.5 illumination.

TABLE 1: PL Decay Times of Polymer Blends Deposited from Different Solvents[a]

sample	emission at (nm)	annealing	τ_1 (ns)	τ_2 (ns)	τ_3 (ns)	average τ (ns)
TCB/CF-cast	600	N	0.07 (48%)	0.88 (28%)	3.9 (24%)	1.2
		Y	0.06 (60%)	0.75 (21%)	3.4 (20%)	0.9
	700	N	0.16 (12%)	2.0 (59%)	6.1 (29%)	3
		Y	0.13 (16%)	1.7 (51%)	5.2 (33%)	2.6
CF-cast	600	N	0.13 (17%)	1.55 (44%)	5.3 (39%)	2.8
		Y	0.06 (42%)	0.81 (29%)	3.6 (29%)	1.3
	700	N	0.6 (8%)	3.3 (76%)	9.5 (16%)	4.1
		Y	0.17 (11%)	2.0 (61%)	5.8 (28%)	2.9

[a] The values are obtained by the best fit to the PL transients after deconvolution of the instrumental response function. The average life times, calculated as the arithmetic means of the decay times weighted with the respective yields, are listed in the last column.

phase separation in these samples is sufficiently large to allow a considerable fraction of excitons formed on the donor to decay radiatively (before reaching the D−A heterojunction). The short decay component is almost absent in the as-prepared blend coated from CF, meaning that excitons formed initially on M3EH-PPV are almost immediately quenched, implying that the exciton diffusion length is very short in these blends. A conclusive assignment of the longer emission decays at 600 nm is rather difficult, but it is not unlikely that these components are due to excitons regenerated from thermally excited exciplexes.

3.5. Photovoltaic Properties. The photovoltaic characteristics of solar cells prepared from CF or the TCB/CF mixture are shown in Figure 7 and the relevant parameters are listed in Table 2. The performance of the as-prepared device made from CF is rather poor, with a maximum IPCE of only 4.5%, an FF of 24% and an ECE of only 0.15%. In contrast, devices coated from the solvent mixture perform quite well, even in the nonannealed state. Upon annealing, the IPCE of the CF-cast device improves by a factor of 4, while it changes only little for samples deposited from the mixed solvent. As shown before for blends coated from CB, there is a strict anticorrelation between the exciplex emission contribution in the steady-state PL and the photovoltaic performance.[12] This suggests that the photovoltaic properties are essentially determined by processes on the local scale, namely the dissociation and recombination of polaron pairs formed at the donor−acceptor heterojunction.

There is a remarkable effect of the preparation conditions on the FF. The annealed blend prepared from TCB/CF exhibits an FF of 44%, which is among the highest values reported for polymer−polymer blends. In contrast, the FF of the as-prepared layer coated from CF is only 24%, implying a large dependence of the photocurrent on the internal electric field. As pointed out above, low fill factors have been attributed to the dependence of free charge carrier generation on the internal electric field, bimolecular recombination of charges before they are extracted at the electrodes, or the formation of space charge due to unbalanced transport.[34] A direct way to distinguish between these processes is to investigate the dependence of photocurrent on the incident light intensity. A well-accepted conclusion is that, for non space-charge-limit devices and negligible bimolecular recombination, the photocurrent should closely follow a linear dependence on light intensity.[35]

Shown in the left graph of Figure 8 are current voltage characteristics of a CF-cast as-prepared device recorded under

TABLE 2: Photovoltaic Parameters of the Samples Shown in Figure 7[a]

sample	annealing	IPCE	V_{oc} (V)	J_{sc} (mA/cm2)	FF	ECE
TCB/CF-Cast	N	31%	1.33	2.1	37%	1.0%
	Y	33%	1.31	2.5	44%	1.42%
CF-Cast	N	4.5%	1.38	0.45	24%	0.15%
	Y	24%	1.29	1.85	26%	0.62%

[a] Incident photon-to-converted electron efficiency (IPCE), open circuit voltage (V_{oc}), short circuit current density (J_{sc}) fill factor (FF), and energy conversion efficiency (ECE).

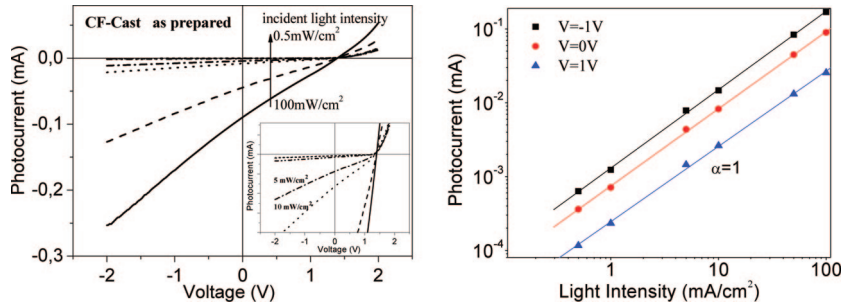

Figure 8. Left: Photocurrent−voltage characteristic of an as-prepared CF-cast sample measured under white light of different intensity. The inset is a closer view for low light intensity. Right: dependence of the photocurrent on the incident light intensity for the same sample with the external bias set at −1 V, 0 V, and 1 V. The solid lines are linear fits with a slope of 1.0.

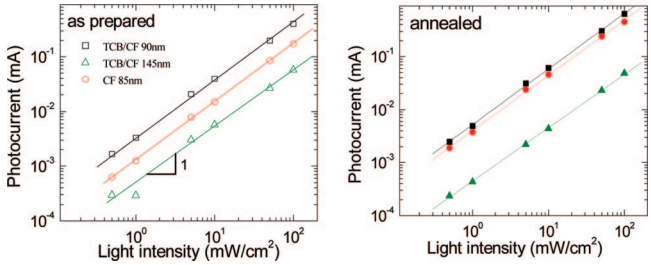

Figure 9. Dependence of the photocurrent on incident light intensity (measured at a bias of −1 V) for M3EH-PPV:CN-ether-PPV blends prepared from TCB/CF (1:4) with an active layer thickness of 90 nm (square) or 145 nm (triangle). Also shown are data for a 85 nm thick blend coated from CF (circles).

different illumination conditions. Apparently, the shape of photocurrent curve does not vary with light intensity, implying that it is not affected by the amount of charges present in the device. Moreover, the photocurrent increases strictly linearly with the incident light intensity, irrespective of the applied voltage (right graph in Figure 8). As shown in Figure 9, all other devices also showed the same strict linear dependence of the photocurrents on light intensity, irrespective of the active layer thickness. No difference in the intensity dependence of photocurrent between annealed and as-prepared samples was observed. These findings rule out space charge formation and bimolecular recombination and imply that the photovoltaic performance is determined by the field-dependence of charge carrier generation. These conclusions are in full agreement with the results of our previous study on the same polymer blend system deposited from chlorobenzene (CB).[12]

In Figure 10, the dark-corrected photocurrents are plotted as a function of the internal electric field $(V_0 - V)/d$ (where V_0 is the compensation voltage at which the photocurrent is equal to zero). The photocurrent of all devices follow a nearly linear dependence up to an electric field of ca. 5×10^6 V/m (corresponding to an external bias of ca. 1 V for an active layer thickness of 60 nm), which can be explained by the competition between drift and diffusion.[14] At higher fields, the as-prepared CF-cast film exhibits the steepest rise (with no clear tendency to saturate), implying that the formed electron−hole pairs are strongly bound.

Charge carrier generation in low mobility solids has been mostly described by either Onsager's model[36] or by the more recent model developed by Braun.[37] Both models rely on the field-induced separation of a Coulombically bound electron−hole pair with initial distance r_o. Though Braun's model appears to be more applicable for disordered organic semiconductors (as it takes into account the recombination of the initially formed charge carriers), we were not able to fit the photocurrent data by assuming a delta-distribution of the initial pair distances r_o. Instead, reasonable fits were obtained over a wide field range when using Onsager's model with a fixed pair distance:

$$\eta(E) = \eta_0 \cdot \frac{1}{2\beta r_0} \cdot e^{-A} \sum_{m=0}^{\infty} \frac{A^m}{m!} \sum_{n=0}^{\infty} \times \left[1 - e^{-2\beta r_0} \sum_{\hbar=0}^{m+n} \frac{(2\beta r_0)^k}{k!}\right]$$

where

$$A = \frac{e^2}{4\pi\varepsilon_0\varepsilon_r k_B T r_0}$$

$$\beta = \frac{eE}{2k_B T}$$

Here η_0 is primary quantum yield, E is the applied field, ε_0 is the vacuum permittivity, and ε_r is dielectric constant of the material.

These fits are shown in Figure 10 as solid and dashed lines. A good agreement to the data at high fields was obtained with an initial separation distances r_0 of 6 nm for the TCB/CF-cast as-prepared sample and $r_0 = 7.1$ nm for the annealed layer. For the CF-coated blend, $r_0 = 3.5$ nm for the as-prepared blend, and $r_0 = 5.6$ nm for the annealed sample. We are well aware of the fact that the value of r_0 retrieved from Onsager's model is not equal to the true initial electron−hole pair radius, but it is, nevertheless, a reasonable measure for the spatial extent of the Coulombically bound polaron pair. It is, therefore, interesting to compare values of r_0 determined for our blends with those reported for conjugated polymers in the literature. When applied to the field-dependent bulk photogeneration in layers of soluble and fully conjugated PPV derivatives such as poly(phenylimino-1,4-phenylenevinylene-2,5-dioctyloxi-1,4-phenylenevinylene-1,4-phenylene) (PA-PPV), poly(methylimino-1,4-phenylene-1-phenyl-1,2-ethenylene-2,5-dimethoxy-1,4-phenylene-2-phenyl-1,2-ethenylene-1,4-phenylene (PPV-amine), or poly[2-methoxy-5-(2′-ethyl-hexyloxy)-1,4-phenylene vinylene] (MEH-PPV), the fit with Onsager's theory yielded r_0 in the range of 1.9 to 2.5 nm.[38,39] This is considerably larger than values reported for polymers with saturated backbone such as polyvinylcarbazole.[40] It indicates that the polaron pair radius of fully conjugated polymers accounts in part for the delocalization of the hole along the polymer backbone. In fact, inserting an ether linkage into the conjugated PPV backbone significantly reduced r_0 to 1.1−1.6 nm.[38] When adding a small amount of C_{60} fullerene to PA-PPV, r_0 increased only slightly (although the photogeneration efficiency increased substantially). This is well understandable, having in mind that the electrons remain localized on the isolated electron acceptors. Lloyd-Hughes and co-workers have

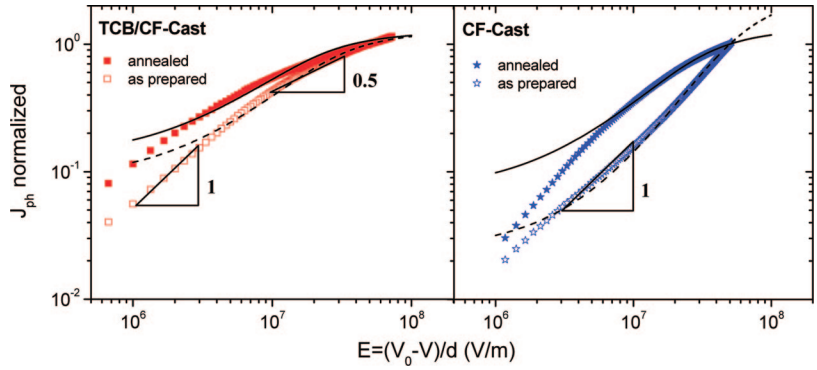

Figure 10. Field dependence of the dark-corrected photocurrent (plotted on a log−log scale) for M3EH-PPV:CN-ether-PPV blends prepared from a 1:4 mixture of TCB/CF (squares) and from pure CF (stars). The photocurrents are normalized to the value at a field of 5×10^7 V/m. Open and full symbols show data for as-prepared and annealed samples, respectively. Dashed and solid lines display the corresponding fits with Onsager's theory as described in detail in the text.

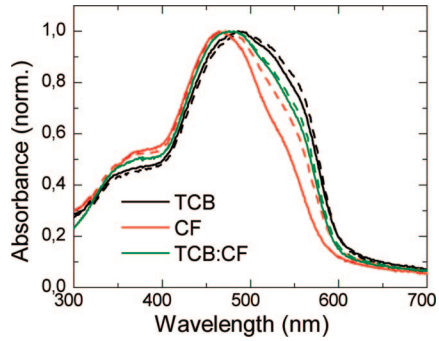

Figure 11. Normalized absorption spectra of 1:1 polymer blends coated from TCB, CF, or a 1:4 TCB/CF solvent mix. Solid and dashed lines are for as-prepared and annealed samples, respectively.

successfully applied Onsager's model to fit the field-dependent efficiency of photoinduced charge generation in an organic field effect transistor made from the conjugated polymer poly[(9,9-dioctylfluorene-2,7-diyl)-*co*-(bithiophene)] (F8T2).[41] Their analysis yielded a polaron pair radius of ca. 2.2 nm, similar to values given above for fully conjugated PPV. The analysis of PL quenching in an as-prepared CF-coated blend of PFB with F8BT yielded $r_0 = 3.1$ at room temperature,[27] which is quite comparable to an electron−hole radius of 3.5 nm determined for our highly intermixed M3EH-PPV/CN-ether-PPV blend prepared under comparable conditions. These values seem to be indicative for a weak delocalization of electrons and holes in an interpenetrating network of donor and acceptor chains. The much higher initial pair radii for our annealed blends, therefore, suggests that carrier generation occurs at the boundary between two rather pure phases of well-organized chains, allowing for the rapid dissociation of the photogenerated polaron pairs. Further evidence for improved chain packing in the annealed blends comes from the absorption spectra of the blend layers, as shown in Figure 11. These spectra show a well-resolved shoulder at the long wavelength side of the blend absorption, which becomes more pronounced and red-shifted upon annealing.

3.6. Mobility and Bimolecular Recombination. Investigations on charge transport and recombination were performed for several reasons. First, recent Monte Carlo simulations based on Onsager's theory suggested a correlation between the carrier mobility and the efficiency for the dissociation of the interfacial polaron pairs.[42] Second, Mandoc and co-workers pointed out that the field-dependent rate of carrier dissociation should be linear in the bimolecular recombination coefficient γ, which itself is a linear function of the average mobility of the electrons and holes.[34] Finally, the good fit of Onsager's model to our field-dependent photocurrent data suggests that dissociation involves the diffusion of both carrier under the influence of their mutual Coulombic potential and the internal electric field. Under these conditions, the bimolecular recombination of carriers should be Langevin-type, with the recombination coefficient given by

$$\gamma_L = \frac{e(\mu_e + \mu_h)}{\varepsilon_0 \varepsilon_r}$$

Here, μ_e and μ_h are the mobility of the electron and hole, respectively. We used the method of "carrier extraction by linearly increasing voltage technique" (photo-CELIV)[43−45] to investigate the transport as well as the rate of bimolecular recombination of charge carriers in the very same polymer blends as used in the solar cell devices. For these measurements, aluminum top electrodes were used instead of Ca/Al to reduce the efficiency for electron injection from the cathode into the blend layer. Charge carries were photogenerated with a ca. 20 ns pulse at 355 nm from a frequency-tripled Nd:YAG laser. Hereby an increased carrier density is generated in the polymer film. During and after excitation, an external forward bias voltage $U_{bias} = -U_{bi}$ was applied to compensate the built-in potential U_{bi} of the sample, resulting in a near-zero electrical field inside the polymer layer. The built-in potential was taken at the point where the photocurrent is equal to zero, in this case $U_{bi} = -0.84$ V. After a waiting time t_d, the photogenerated charges were extracted by linearly increasing the applied reverse voltage up to ~10 V within several microseconds. The extracted current densities were monitored by a digital oscilloscope and feature a single maximum with amplitude j_{max} at delay time t_{max} after starting the extraction voltage ramp (see Figure 11). From the measured current transients, the charge mobility can be calculated as $\mu = 2d^2[3t_{max}^2(1 + 0.18\Delta j/j_{cap})\mathrm{d}E/\mathrm{d}t]^{-1}$, where E is the electric field, $j_{cap} = \varepsilon\varepsilon_0(\mathrm{d}E/\mathrm{d}t)$ is the capacitive charging current and $\Delta j = j_{max} - j_{cap}$.[46−48] The charge density left after the delay time t_d can be approximately calculated from $n = \epsilon\epsilon_0/(e\mu j_{cap})j'(t_d)$, where e is the elementary charge and $j'(t_d)$ is the derivative of the current at time t_d.[47] Figure 12 shows typical photo-CELIV current transients for varying values of t_d. For all sample types, we found a reduction of j_{max} and an increase of t_{max} upon increasing t_d, corresponding to a drop in mobility. The obtained mobilities and extracted charge densities for TCB/CF and CF cast samples are shown in Figure 13. All samples show a strong decrease of the mobility during the first 10 μs after photoexcitation. Mobility relaxation by around 40% within the first 10 μs after photogeneration of carriers has previously

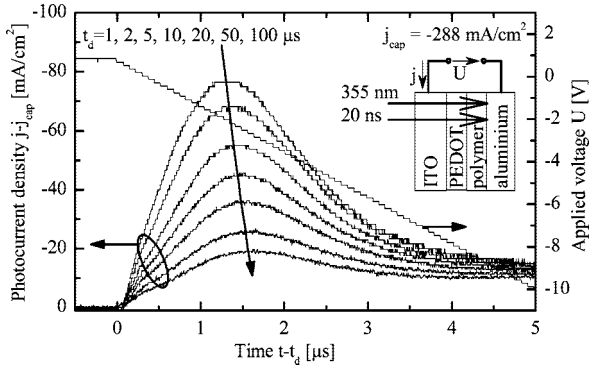

Figure 12. Typical photocurrent transients obtained from a CB-cast blend film with a thickness of $d = 53$ nm and an active area of 1 mm^2 at $dE/dt = 4 \times 10^{13}$ V m^{-1} s^{-1}. The delay time t_d between photoexcitation and carrier extraction is varied from 1 to 100 μs. The inset schematically shows the sample layer structure, the electrical circuit, and the illumination direction. The top-down arrow represents the corresponding t_d parameter to each curve oriented toward increased delay times.

been reported by Mozer et al.[45] for (poly[2-methoxy-5-(3,7-dimethyloctyloxy)]-1,4-phenylenevinylene) (MDMO-PPV) and PCBM blend solar cells using the same method. They attributed this to an energetic relaxation of charge carriers. In addition, the extracted charge density decreases largely with increasing waiting time t_d. During this time period, the internal field is nearly zero and the photogenerated charge density decays exclusively via bimolecular recombination.

Mobilities and bimolecular recombination coefficients determined from the regimes immediately following or at longer times after photoexcitation are summarized in Table 3. It should be pointed out that CELIV measurements do not differentiate between the types of charge carriers. Hence, the results cannot be ascribed directly to either the motion of holes or electrons. Note that the mobilities deduced from our experiments are approximately 1 order of magnitude higher than the zero-field mobility measured for a related electron-accepting polymer by Mandoc and co-workers.[49] This suggests that the extraction signal seen in our CELIV experiment is due to holes, and that these are the faster carriers.

The conclusion can be drawn that films prepared from different solvents show similar hole mobilities and no significant improvement is observed upon annealing. Moreover, the bimolecular recombination coefficient (and the value of the effective mobility μ_{eff} as derived from this) is the same for all blends within the range of batch-to-batch variations (not shown). The effective mobility as deduced from the bimolecular recombination, assuming Langevin-type recombination is a factor of 2−4 lower than the (hole) mobility determined from the maximum in the extraction transients. Note that the bimolecular recombination is measured at zero internal fields, while the maximum of the extraction current appears at a field of ca. 4×10^7 V/m. Taking into account that the charge mobility generally increases with field, one can conclude that bimolecular recombination is nearly Langevin-type. Non-Langevin recombination has been rarely observed, e.g., in highly phase-separated blends of poly(3-hexylthiophene) and soluble fullerene.[50] Our measurements show that the process underlying charge carrier recombination and separation in our samples is diffusion controlled in all cases, despite different degrees of phase separation and significant differences in the photovoltaic properties.

4. Conclusion

We reported a detailed study on how the charge carrier generation and the radiative recombination of intrachain versus interchain excitations can be tuned in M3EH-PPV/CN-ether-PPV (1:1 by weight) blends. By using pure solvents as well as the respective solvent mixtures for film deposition, a great variety of blend morphologies was achieved. Information on the blend morphology came from steady-state and time-resolved fluorescence studies. As-prepared layers coated from CF exhibited only emission from the exciplexes formed at the donor−acceptor heterojunction, with no evidence for the radiative decay of either the M3EH-PPV or the CN-ether-PPV exciton. Evidently these intrachain excited species dissociate rapidly by intermolecular charge transfer, pointing to a highly intermixed blend morphology. By using a poor solvent TCB for M3EH-PPV, which is concomitantly a good one for CN-ether-PPV, phase-separation at an early stage of film deposition was induced. The appearance of emission from the M3EH-PPV exciton suggests that this morphology contains nanosized domains composed almost entirely of the donor polymer. However, we found no emission from either the CN-ether-PPV exciton or the excimer in any of our blend layers. Hence we lack information on whether phase separation leads to pure acceptor phases. Nevertheless, the rather high polaron pair radius as deduced from the Onsager fit suggests that both kinds of carriers are well delocalized on their respective phases in the phase-separated blends. Our view of the correlation between the morphology and excited-state properties is summarized in Figure 14.

The nanomorphology is shown to have a large influence on the external quantum efficiency and particularly on the shape of the photocurrent characteristics. While as-prepared layers coated from CF exhibited fill factors of less than 25%, an FF of 44% was measured for annealed blends coated from the TCB/CF blend. The latter value is among the highest reported for polymer−polymer solar cells. The strict linear relation of photocurrent and incident light intensity rules out space charge effects and bimolecular recombination as the main factors determining the device properties. Photo-CELIV measurements confirmed that the variation in the performance of devices prepared under different conditions can be related to neither differences in the bulk mobilities nor significant changes of the (zero-field) bimolecular recombination coefficient.

The findings strongly support our earlier conclusions that the photovoltaic properties are determined by processes on the very local scale, namely the competition between the field-induced dissociation and recombination of the initially formed polaron pair. We propose that the nanomorphology mainly affects the way how the kinetic energy of the electron injected into the acceptor phase following exciton break-up at the heterojunction is used to decrease its mutual Coulombic binding energy with the hole remaining on the donor phase (and vice versa). The kinetics of this process is expected to depend on the direct environment of the electron-accepting chains. Moreover, it might be well reduced if the density of electron-transporting sites is lowered by the presence of donor chains in intermixed acceptor-rich phases, leading to tightly bound polaron pairs. Those pairs will be more vulnerable to recombination via the formation of inter-
facial exciplexes or possibly via intrachain triplet excitons.[29,51,52] In contrast to this, rather pure donor and acceptor phases will favor the formation of spatially extended interfacial electron−hole pairs, which exhibit a high probability to escape from their mutual Coulombic potential.

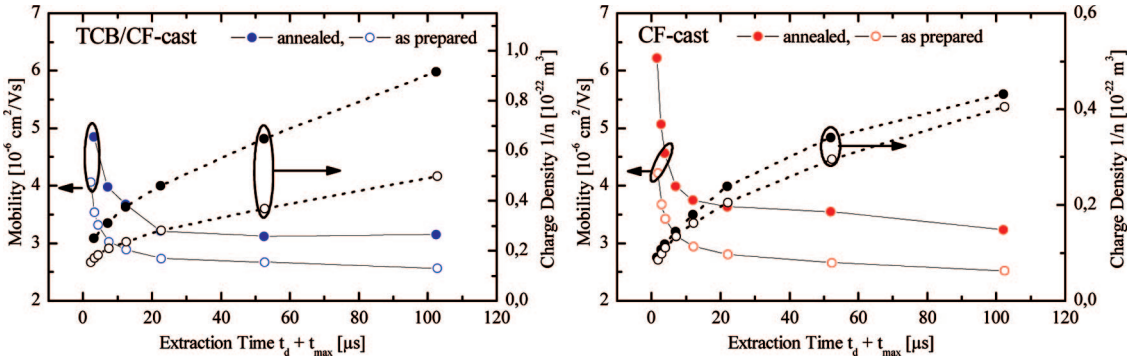

Figure 13. Charge mobility values from CELIV experiments as a function of the delay time t_d between excitation and charge extraction. The charge density as a function of t_d is also given.

TABLE 3: Charge Mobilities and Bimolecular Recombination Coefficients of M3EH-PPV:CN-ether-PPV Blend Layers with Different Preparation Conditions

			derived from transient peak				derived from charge recombination	
sample	annealing	thickness (nm)	μ (short)[a] (cm^2/V s)	μ (long)[a] (cm^2/V s)	γ (short)[b] (m^3/s)	γ (long)[b] (m^3/s)	μ_{eff} (short)[c] (cm^2/V s)	μ_{eff} (long)[c] (cm^2/V s)
			M3EH-PPV:CN-ether-PPV blends					
CF	N	55	4.2e-6	2.5e-6	9.2e-19	2.7e-19	1.5e-6	4.4e-7
CF	Y	55	6.2e-6	3.2e-6	9.9e-19	2.4e-19	1.7e-6	3.9e-7
TCB/CF	N	65	4.1e-6	2.6e-6	1.0e-18	2.9e-19	1.7e-6	4.7e-7
TCB/CF	Y	65	4.8e-6	3.1e-6	1.2e-18	5.9e-19	2.1e-6	9.7e-7

[a] Mobility of charge carriers obtained from the transient peak during applied electric field at short time scale (1−10 μs) and at long time scale (10−100 μs). [b] γ is the zero-field bimolecular recombination coefficient, which is obtained from the slope of inversed charge density vs extraction time. Since the curve is not a straight line, the γ we used here is derived from the short time and long time scales, respectively. [c] μ_{eff}: effective mobility, which is calculated as $\mu_{eff} = \varepsilon_0\varepsilon_r\gamma/e$.

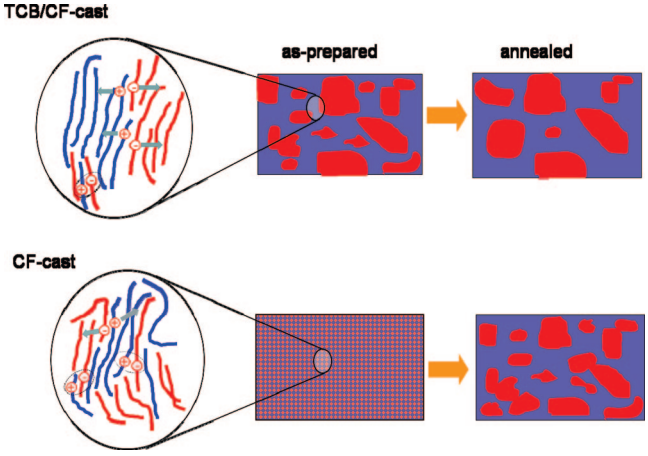

Figure 14. Proposed nanomorphology for TCB/CF-cast and CF-cast films, before and after annealing. The close view is a simplified picture of charge carrier generation and exciplex formation in relation to the degree of phase separation.

These conclusions are in full agreement with recent Monte Carlo simulations on nanostructured blends by Marsh and coworkers.[53] These simulations predicted the geminate recombination efficiency to decrease from ca. 85% for a blend with a feature size of 2.5 nm to 70% for a domain size of 5.8 nm. At the same time, the carrier collection efficiency was shown to increase remarkably. A second important conclusion of these simulations was that the bulk charge transport is barely affected by the typical domain size. This prediction agrees well with the results of our CELIV measurements and the conclusions drawn from the experiments on single-carrier devices.[15,16]

We would finally like to note that changing the morphology by the use of different solvents (or annealing the sample) does not affect the principle mechanism of charge carrier photogeneration, which involves the diffusive motion of carriers under the action of the mutual Coulombic potential and the internal electric field. This is clearly evident from the close-to-Langevin-type carrier recombination and the Onsager-type field-dependency of the photocurrent. This field dependence sets a fundamental limit to the FF and consequently to the overall solar cell efficiency. It has been pointed out that a weaker field dependence of the photogeneration efficiency necessitates a reduction of the coefficient for bimolecular recombination well below the Langevin limit.[54] As stated above, strongly reduced recombination coefficients have been rarely observed in all-organic devices, e.g., in the blend of P3HT (poly(3-hexylthiophene)) with PCBM.[50] These blends were shown to exhibit large single crystalline domains of PCBM embedded into a polymer-rich matrix. Further efforts to improve the efficiency of polymer−polymer solar cells must, therefore, focus on the formation of interpenetrating bicontinuous networks from highly ordered polymer domains, allowing the photogenerated holes and electrons to move independently in two different phases.

Acknowledgment. This work was supported by the Volkswagen Foundation and the state of Brandenburg by the graduate school "Confined reactions and interactions in soft matter systems". We thank Prof. Dr. Österbacka (Abo Akademi University, Finland) and Dr. A. Pivrikas (Johannes Kepler Univerity) for their comments on bimolecular recombination in low mobility solids. Dr. C. Dosche and Prof. Dr. H.-G. Löhmannsröben, (University of Potsdam) are acknowledged for access to the setups for time-resolved luminescence measurements.

References and Notes

(1) Halls, J. J. M.; Walsh, C. A.; Greenham, N. C.; Marseglia, E. A.; Friend, R. H.; Moratti, S. C.; Holmes, A. B. *Nature* **1995**, *376*, 498.
(2) Yu, G.; Heeger, A. J. *J. Appl. Phys.* **1995**, *78*, 4510.

(3) Yu, G.; Gao, J.; Hummelen, J. C.; Wudl, F.; Heeger, A. J. *Science* **1995**, *270*, 1789.
(4) Kietzke, T.; Hörhold, H.-H.; Neher, D. *Chem. Mater.* **2005**, *17*, 6532.
(5) Koetse, M.; Sweelssen, J.; Hoekerd, K.; Schoo, H. F. M.; Veenstra, S. C.; Kroon, J. M.; Yang, X.; Loos, J. *Appl. Phys. Lett.* **2006**, *88*, 083504.
(6) McNeill, C. R.; Abrusci, A.; Zaumseil, J.; Wilson, R.; McKiernan, M. J.; Burroughes, J. H.; Halls, J. J. M.; Greenham, N. C.; Friend, R. H. *Appl. Phys. Lett.* **2007**, *90*, 193506.
(7) Li, G.; Shrotriya, V.; Huang, J.; Yao, Y.; Moriarty, T.; Emery, K.; Yang, Y. *Nat. Mater.* **2005**, *4*, 864.
(8) Kim, S.-S.; Na, S.-I.; Jo, J.; Tae, G.; Kim, D.-Y. *Adv. Mater.* **2007**, *19*, 4410.
(9) Kim, K.; Liu, J.; Namboothiry, M. A. G.; Carroll, D. L. *Appl. Phys. Lett.* **2007**, *90*, 163511.
(10) Schilinsky, P.; Waldauf, C.; Huach, J.; Brabec, C. J. *J. Appl. Phys.* **2004**, *95*, 2816.
(11) Kietzke, T.; Egbe, D. A. M.; Hörhold, H.-H.; Neher, D. *Macromolecules* **2006**, *39*, 4018.
(12) Yin, C.; Kietzke, T.; Neher, D.; Hörhold, H. H. *Appl. Phys. Lett.* **2007**, *90*, 092117.
(13) Yin, C.; Pieper, B.; Stiller, B.; Kietzke, T.; Neher, D. *Appl. Phys. Lett.* **2007**, *90*, 133502.
(14) Mihailetchi, V. D.; Koster, L. J. A.; Hummelen, J. C.; Blom, P. W. M. *Phys. Rev. Lett.* **2004**, *93*, 216601.
(15) Mandoc, M. M.; Veurman, W.; Sweelssen, J.; Koetse, M. M.; Blom, P. W. M. *Appl. Phys. Lett.* **2007**, *91*, 073518.
(16) McNeill, C. R.; Westenhoff, S.; Groves, C.; Friend, R. H.; Greenham, N. C. *J. Phys. Chem. C* **2007**, *111*, 19153.
(17) Halls, J. J. M.; Arias, A. C.; MacKenzie, J. D.; Wu, W. S.; Inbasekaran, M.; Woo, E. P.; Friend, R. H. *Adv. Mater.* **2000**, *12*, 498.
(18) Shaheen, S. E.; Brabec, C. J.; Sariciftci, N. S.; Padinger, F.; Fromherz, T.; Hummelen, J. C. *Appl. Phys. Lett.* **2001**, *78*, 841.
(19) Peet, J.; Kim, J. Y.; Coates, N. E.; Ma, W. L.; Moses, D.; Heeger, A. J.; Bazan, G. C. *Nat. Mater.* **2007**, *6*, 497.
(20) Moule, A. J.; Meerholz, K. *Adv. Mater.* **2008**, *20*, 240.
(21) *Hazardous Substances Data Bank*; U.S. Department of Health and Human Services: Bethesda, MD, 1993.
(22) Chang, J.-F.; Sun, B.; Breiby, D. W.; Nielsen, M. M.; Solling, T. I.; Giles, M.; McCulloch, I.; Sirringhaus, H. *Chem. Mater.* **2004**, *16*, 4772.
(23) Kumke, M. In *Mathematisch-Naturwissenschaftlichen Fakultät*; Universität Potsdam: Potsdam, Germany, 2005; p 215.
(24) Chasteen, S. V.; Härter, J. O.; Rumbles, G.; Scott, J. C.; Nakazawa, Y.; Jones, M.; Hörhold, H.-H.; Tillman, H.; Carter, S. A. *J. Appl. Phys.* **2006**, *99*, 033709.
(25) Chasteen, S. V.; Carter, S. A.; Rumbles, G. *J. Chem. Phys.* **2006**, *124*, 214704.
(26) Yin, C.; Kietzke, T.; Kumke, M. U.; Neher, D.; Hörhold, H.-H. *Sol. Energy Mater. Sol. Cells* **2007**, *91*, 411.
(27) Morteani, A. C.; Sreearunothai, P.; Herz, L. M.; Friend, R. H.; Silva, C. *Phys. Rev. Lett.* **2004**, *92*, 247402.
(28) Morteani, A. C.; Dhoot, A. S.; Kim, J.-S.; Silva, C.; Greenham, N. C.; Murphy, C.; Moons, S.; Cina, S.; Burroughes, J. H.; Friend, R. H. *Adv. Mater.* **2003**, *15*, 1708.
(29) Offermans, T.; van Hal, P. A.; Meskers, S. C. J.; Koetse, M. M.; Janssen, R. A. *Phys. Rev. B* **2005**, *72*, 045213.
(30) Veenstra, S. C.; Verhees, W. J. H.; Kroon, J. M.; Koetse, M. M.; Sweelssen, J.; Bastiaansen, J. J. A. M.; Schoo, H. F. M.; Yang, X.; Alexeev, A.; Loos, J.; Schubert, U. S.; Wienk, M. M. *Chem. Mater.* **2004**, *16*, 2503.
(31) Snaith, H. J.; Arias, A. C.; Morteani, A. C.; Silva, C.; Friend, R. H. *Nano Lett.* **2002**, *2*, 1353.
(32) McNeill, C. R.; Frohne, H.; Holdsworth, J. L.; Dastoor, P. C. *Nano Lett.* **2004**, *4*, 2503.
(33) Kietzke, T.; Neher, D.; Kumke, M.; Ghazy, O.; Ziener, U.; Landfester, K. *Small* **2007**, *3*, 1041.
(34) Mandoc, M. M.; Veurman, W.; Koster, L. J. A.; de Boer, B.; Blom, P. W. M. *Adv. Funct. Mater.* **2007**, *17*, 2167.
(35) Mihailetchi, V. D.; Wildemann, J.; Blom, P. W. M. *Phys. Rev. Lett.* **2005**, *94*, 126602.
(36) Onsager, L. *Phys. Rev.* **1938**, *54*, 554.
(37) Braun, C. L. *J. Chem. Phys.* **1984**, *80*, 4157.
(38) Barth, S.; Bässler, H. *Phys. Rev. Lett.* **1997**, *79*, 4445.
(39) Däubler, T. K.; Cimrová, V.; Pfeiffer, S.; Hörhold, H.-H.; Neher, D. *Adv. Mater.* **1999**, *11*, 1274.
(40) Cimrova, V.; Nespurek, S. *Chem. Phys.* **1994**, *184*, 283.
(41) Lloyd-Hughes, J.; Richards, T.; Sirringhaus, H.; Johnston, M. B.; Herz, L. M. *Phys. Rev. B* **2008**, *77*, 1253203.
(42) Offermans, T.; Meskers, S. C. J.; Janssen, R. A. J. *Chem. Phys.* **2005**, *308*, 125.
(43) Österbacka, R.; Pivrikas, A.; Juska, G.; Genevicius, K.; Arlauskas, K.; Stubb, H. *Curr. Appl. Phys.* **2004**, *4*, 534.
(44) Juska, G.; Nekrasas, N.; Genevicius, K.; Stuchlik, J.; Kocka, J. *Thin Solid Films* **2004**, *451*−*452*, 290.
(45) Mozer, A. J.; Sariciftci, N. S.; Lutsen, L.; Vanderzande, D.; Österbacka, R.; Westerling, M.; Juska, G. *Appl. Phys. Lett.* **2005**, *86*, 112104.
(46) Juska, G.; Arlauskas, K.; Viliunas, M.; Genevicius, K.; Österbacka, R.; Stubb, H. *Phys. Rev. B* **2000**, *62*, R16235.
(47) Juska, G.; Arlauskas, K.; Viliunas, M.; Kocka, J. *Phys. Rev. Lett.* **2000**, *84*, 4946.
(48) The equation is derived according to reference 47. Here we corrected the minor error in the corresponding equation given in reference 46.
(49) Mandoc, M. M.; Veurman, W.; Koster, L. J. A.; Koetse, M. M.; Sweelssen, J.; de Boer, B.; Blom, P. W. M. *J. Appl. Phys.* **2007**, *101*, 104512.
(50) Pivrikas, A.; Juška, G.; Mozer, A. J. *Phys. Rev. Lett.* **2005**, *94*, 176806.
(51) Ford, T. A.; Avilov, I.; Beljonne, D.; Greenham, N. C. *Phys. Rev. B* **2005**, *71*, 125212.
(52) Veldman, D.; Offermans, T.; Sweelssen, J.; Koetse, M. M.; Meskers, S. C. J.; Janssen, R. A. J. *Thin Solid Films* **2006**, *511*−*512*, 333.
(53) Marsh, R. A.; Groves, C.; Greenham, N. C. *J. Appl. Phys.* **2007**, *101*, 083509.
(54) Juška, G.; Arlauskas, K.; Stuchlik, J. *J. Non-Cryst. Solids* **2006**, *352*, 1167.

JP803977K